

(Sarnthein, Küssner, Grootes, Ausin, Eglinton, Muglia, Muscheler, and Schlolaut ):

## SUPPLEMENTARY TEXT

### Section 2.2 – *Uncertainties of age control*

Rough estimates of uncertainty and aspects of analytical quality were published by Sarnthein et al. (2007, 2015). We now focus on uncertainties tied to the calendar age definition for each  $^{14}\text{C}$  plateau boundary both in the Suigetsu atmospheric and the various marine sediment records (Table 1). To recap, an age/sediment section is formally defined as containing a ‘ $^{14}\text{C}$  plateau’, when  $^{14}\text{C}$  ages show almost constant values with an overall gradient of  $<0.3$  to  $<0.5$   $^{14}\text{C}$  yr per cal. yr (based on visual description and/or statistical estimates by means of the 1st derivative of all downcore changes in the  $^{14}\text{C}$  age – calendar age relationship; Sarnthein et al., 2015) and a variance of less than  $\pm 100$  to  $\pm 300$   $^{14}\text{C}$  yr, and up to 500  $^{14}\text{C}$  yr prior to 25 cal. ka. Here  $^{14}\text{C}$  ages form a plateau-shaped scatter band with up to 10% outliers, that extends over more than 300 cal. yr in the Suigetsu record and/or equivalent sections of marine sediment depth (following rules defined by Sarnthein et al., 2007).

On visual inspection a plateau boundary is assigned to the break point between the low to zero or reversed slope of a  $^{14}\text{C}$  plateau and the normally high regression slope of the  $^{14}\text{C}$  concentration jump that separates two consecutive plateaus (Figs. 1 and S1). More precisely, a boundary marks the point, where the  $^{14}\text{C}$  curve exceeds the scatter band of the plateau either crossing the upper or lower envelope

line. Thus the boundary is chosen about halfway between the last  $^{14}\text{C}$  age within a plateau band and the next following age outside the scatter band (Figs. 1 and 2). Both on the previously varve-based and the now U/Th-based model age scale (Bronk Ramsey et al., 2012) most  $^{14}\text{C}$  dates of the Lake Suigetsu section are spaced at intervals of <10–60 yr from 10 to 15 cal. ka and ones of 20–140 yr between 15 and 29 cal. ka (Fig. 1). Thus the uncertainty of a plateau boundary age assigned halfway between two  $^{14}\text{C}$  ages nearby inside and outside a plateau's scatter band would, on average, amount to  $\pm 10\text{--}\pm 70$  cal. yr.

In principle, the calendar age uncertainties of marine  $^{14}\text{C}$  plateau boundaries are treated likewise: After being tuned to those in the Suigetsu  $^{14}\text{C}$  record, the uncertainties are deduced for the position of all plateaus of a suite within the uncertainty envelope of the U/Th model-based age calibration. Hence the estimates of total age uncertainty present the square root of the squared uncertainty of the calibrated age of each plateau boundary at Suigetsu plus that of the marine record, where variable depth spacing of  $^{14}\text{C}$  ages is converted into average time spans.

#### CAPTIONS of SUPPLEMENT FIGURES

✓ Fig. S1. Individual atmospheric  $^{14}\text{C}$  ages and error bars of Lake Suigetsu plant macrofossils 15–27 cal. ka vs. U/Th-based model age (blue dots; Bronk Ramsey et al., 2012).  $^{14}\text{C}$  plateaus longer than 250 yr are outlined by a suite of labeled horizontal boxes that envelop scatter bands of largely constant  $^{14}\text{C}$  ages. Red dots and black circles in Fig. 1a display  $^{14}\text{C}$  ages of Hulu stalagmites. Similar to Suigetsu  $^{14}\text{C}$  ages those of Hulu Cave also show a suite

of  $^{14}\text{C}$  plateaus (red boxes) tentatively assigned in this figure, plateaus that are shorter than Suigetsu-based plateaus and occupy slightly different age ranges.

Fig. S1

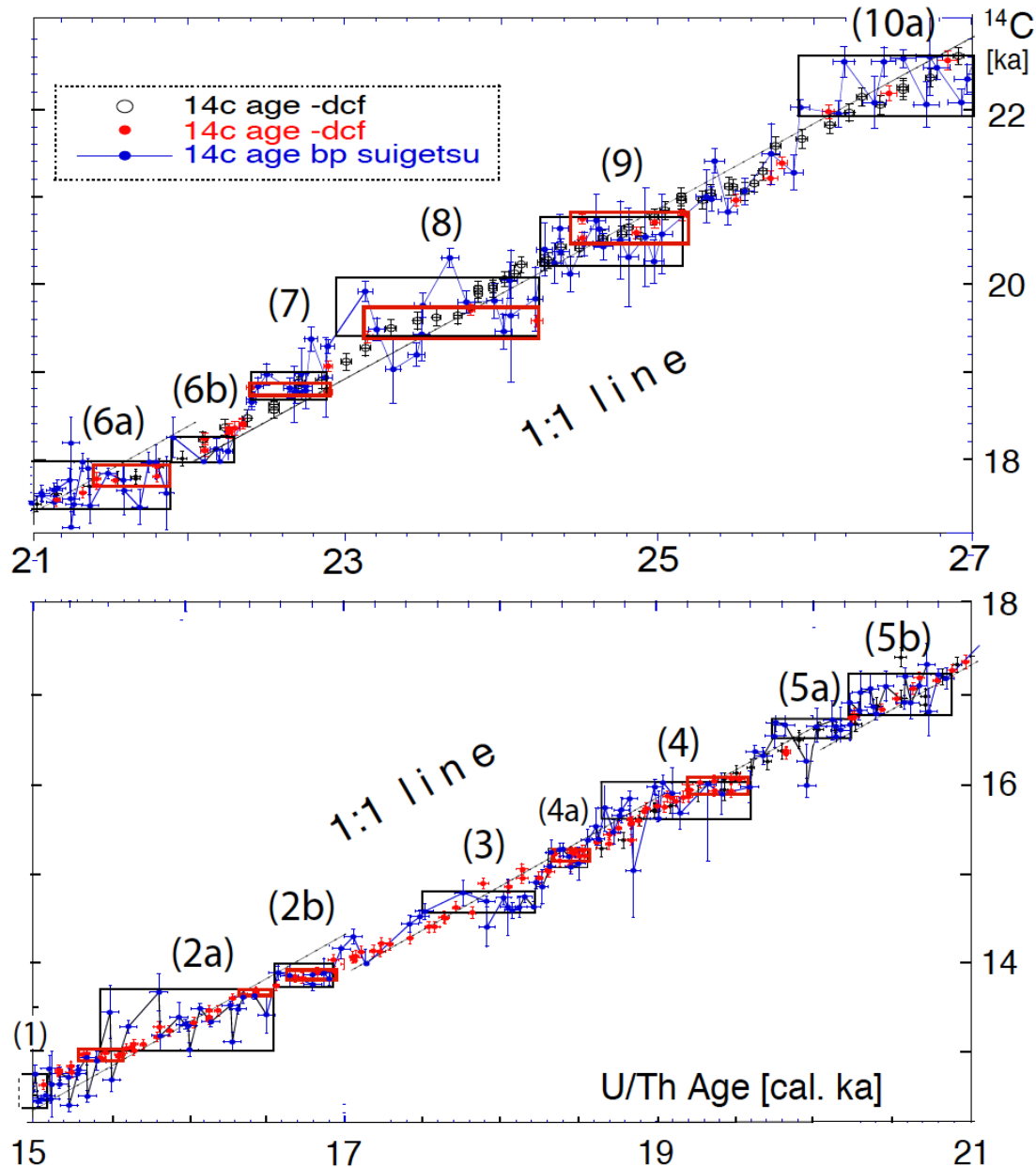


Fig. S2. Location and water depths of sediment cores with age control based on  $^{14}\text{C}$  plateau tuning.  $^{14}\text{C}$  reservoir ages of cores labeled with 'w' are derived from samples with paired wood chunks and planktic foraminifers.

Fig. S2a

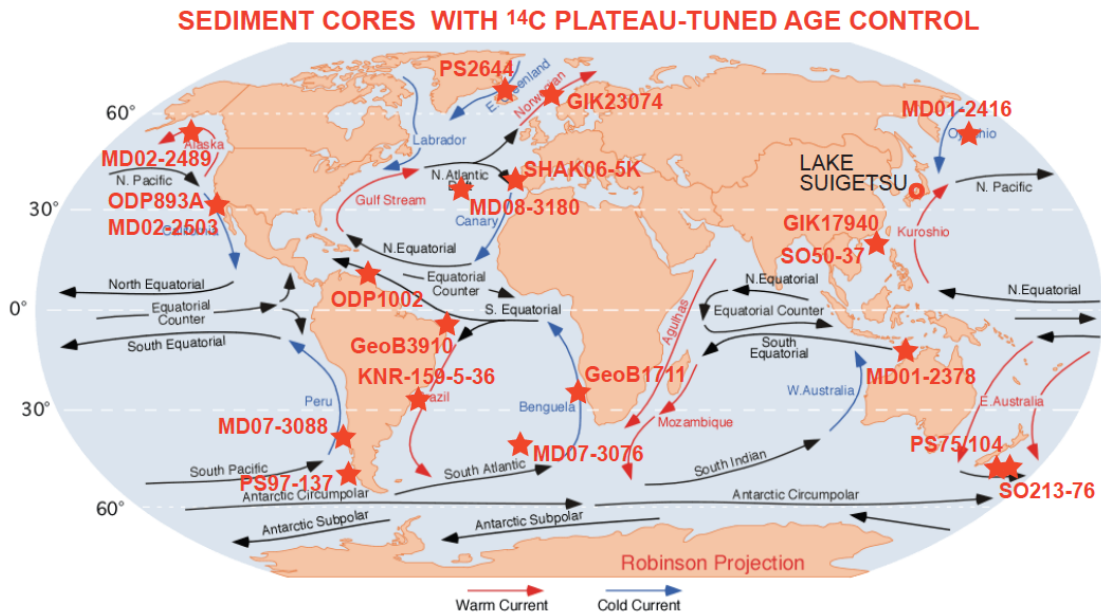
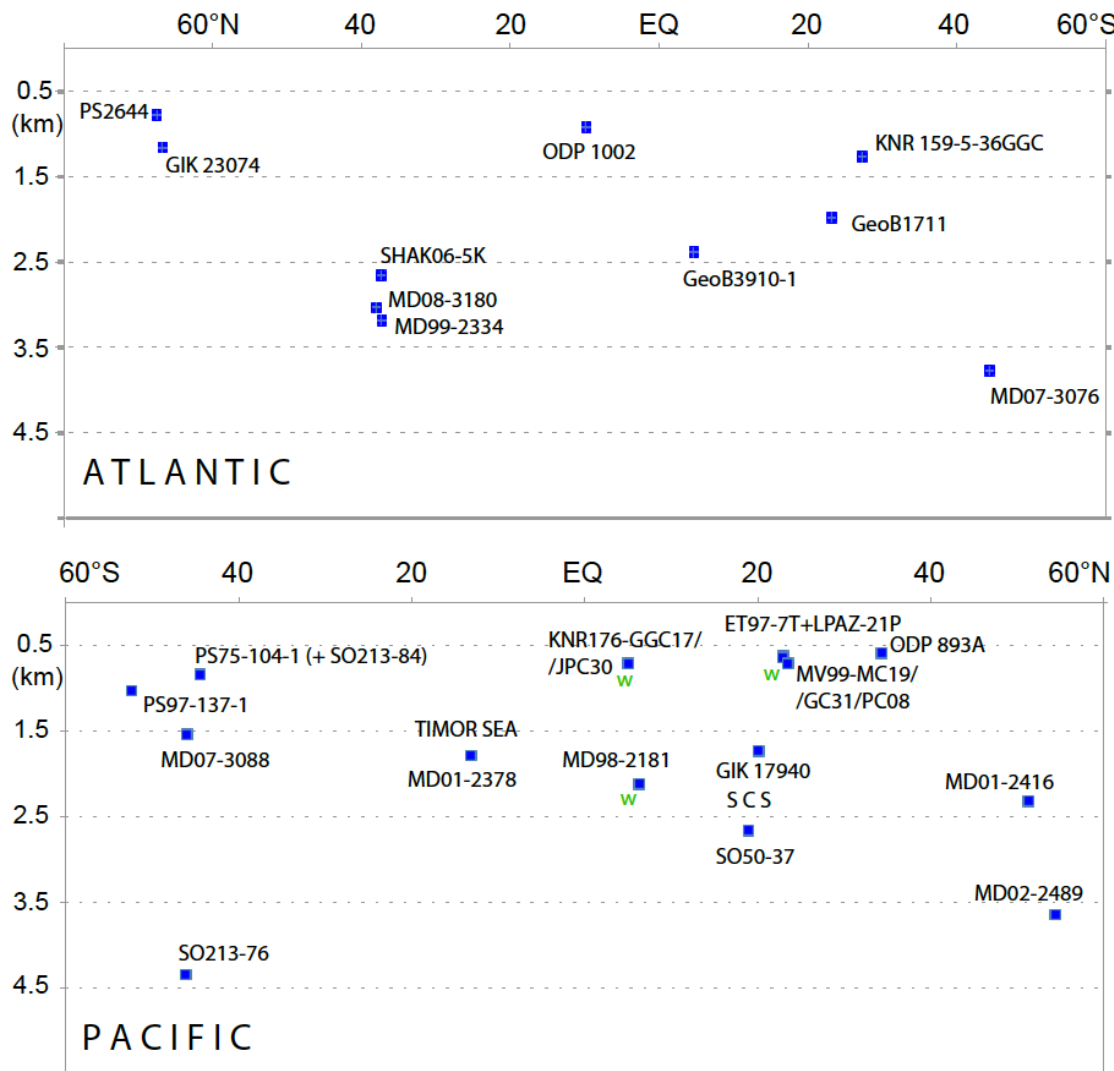


Fig. S2b



↙ Fig. S3. (a) Global distribution of  $^{14}\text{C}$  reservoir ages obtained by  $^{14}\text{C}$  plateau tuning technique for late LGM surface waters, (b) intermediate waters (100–1800 m w.d.) and (c) for ocean deep waters (>1800 m w.d. and Site GIK 23074 at 1157 m in the Norwegian Sea). (d)  $^{14}\text{C}$  reservoir ages of LGM surface waters modeled by Muglia et al. (2018) for sites with plankton-based age values.

Fig. S3a

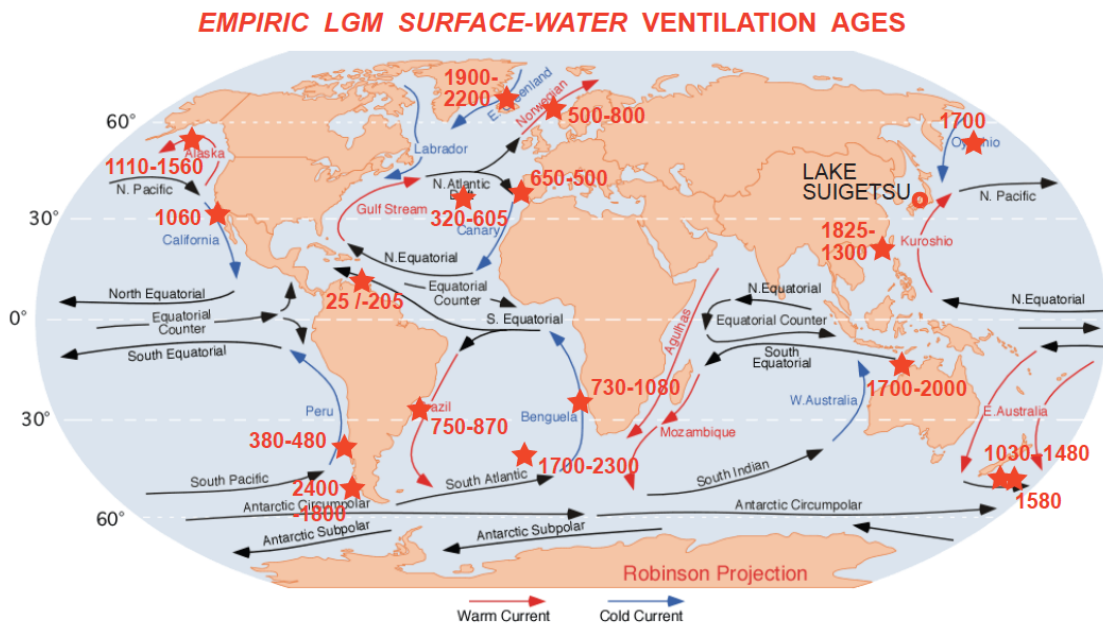


Fig. S3b

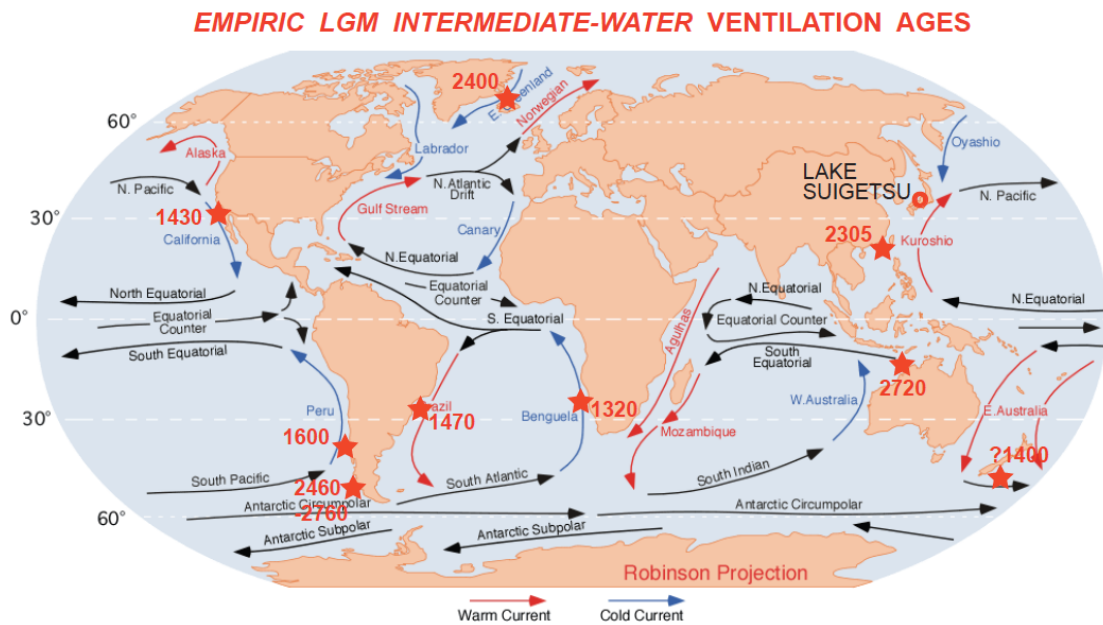


Fig. S3c

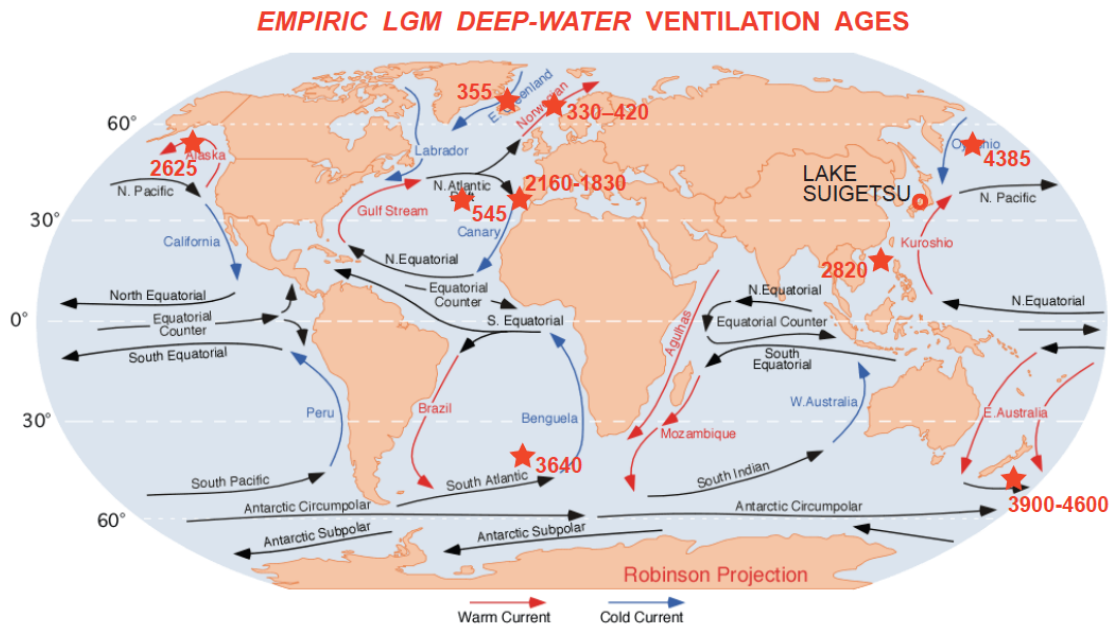
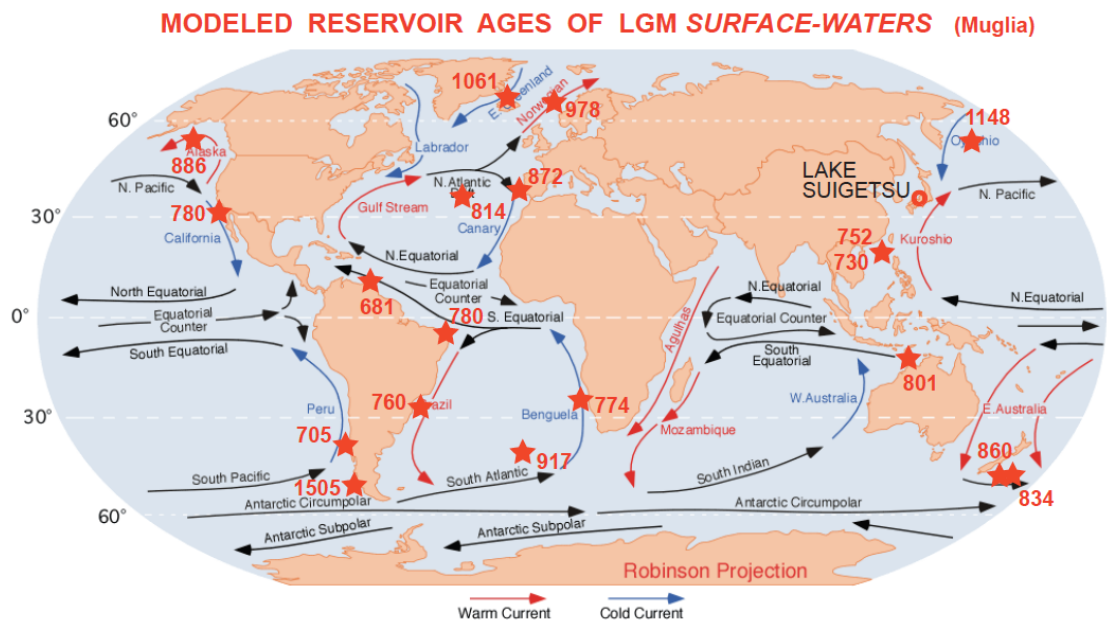


Fig. S3d



✓ Fig. S4. Centennial-to-millennial-scale temporal and spatial variations in planktic (pla.) reservoir (res.) and (raw = uncorrected) apparent (app.) benthic  $^{14}\text{C}$  ventilation (vent.) ages recorded at 18/20 key sites in the Atlantic (S4 a, b, e), Pacific (S4 c, d), and Indian (S4 e). Site locations are given in Fig. S2. Stratigraphic units are marked on top of each diagram: Younger Dryas (YD),

Bølling-Allerød (B/A) Heinrich Stadial 1 (HS-1), Last Glacial Maximum (LGM), and Heinrich Stadial 2 (HS-2).

*Origin and various features characteristic of  $^{14}\text{C}$  records:* About 50% of all planktic and ('raw') benthic  $^{14}\text{C}$  records already were published in Sarnthein et al. (2015). However, the cal. age of all records originally based on microscopy-based varve counts was now converted into U/Th-based model ages (Bronk-Ramsey et al., 2012). Planktic  $^{14}\text{C}$  reservoir ages of Core GIK23074 are now supplemented by benthic ventilation ages. Planktic  $^{14}\text{C}$  reservoir ages of SHAK06-5K are detailed in Ausin et al. (2019, in prep.). Benthic ventilation ages plotted for SHAK06-5K are matched from neighbor core MD99-2334K (Skinner et al., 2014) the stratigraphy and  $^{14}\text{C}$  reservoir ages of which are closely correlated by means of narrow-spaced suites of  $^{14}\text{C}$  ages. To show an example, 'raw' benthic ventilation ages in Core MD08-3180 are recalculated into 'actual' ventilation ages (Balmer and Sarnthein, 2018) that incorporate past changes in atmospheric  $^{14}\text{C}$  concentration between the time of deep-water formation and the local growth of benthic foraminifers. South Atlantic  $^{14}\text{C}$  records GeoB3910, GeoB1711-4, and KNR-159-5-36 (data slightly supplemented) are from Balmer et al. (2016), now however, with cal. ages converted into U/Th based model ages. The same applies to MD07-3076, where the continuous planktic and benthic  $^{14}\text{C}$  records are from Skinner et al. (2010), corroborated by three blue bars reflecting the extent of planktic  $^{14}\text{C}$  plateaus tuned to atmospheric plateaus no. 1, 2b, and 4. South Pacific  $^{14}\text{C}$  records PS75-104, SO213-76, MD07-3088, and PS97-137-1 are from Küssner et al., 2018 and 2019, in prep.). Planktic and benthic  $^{14}\text{C}$  records of neighbor cores GIK17940 and SO50-37, PS75-104 and SO213-84, and ODP893A and

MD02-2503 each are plotted on joint graphs, paired records that are obtained from small-scale sea regions with a common level of planktic  $^{14}\text{C}$  reservoir age. Benthic  $^{14}\text{C}$  ages of SO50-37 and SO213-84 are from Ronge et al. (2016), those of MD07-3088 from Siani et al. (2013).

Fig. S4a. NORTH ATLANTIC AND NORDIC SEA SITES

*WEST and CENTER* —

— *EAST*

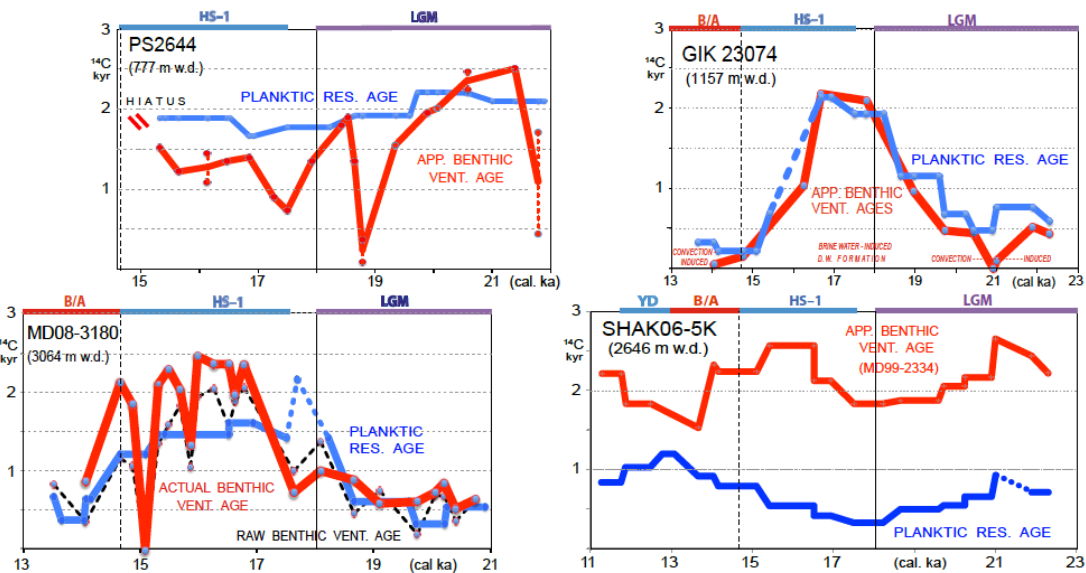


Fig. S4b. SOUTH ATLANTIC SITES

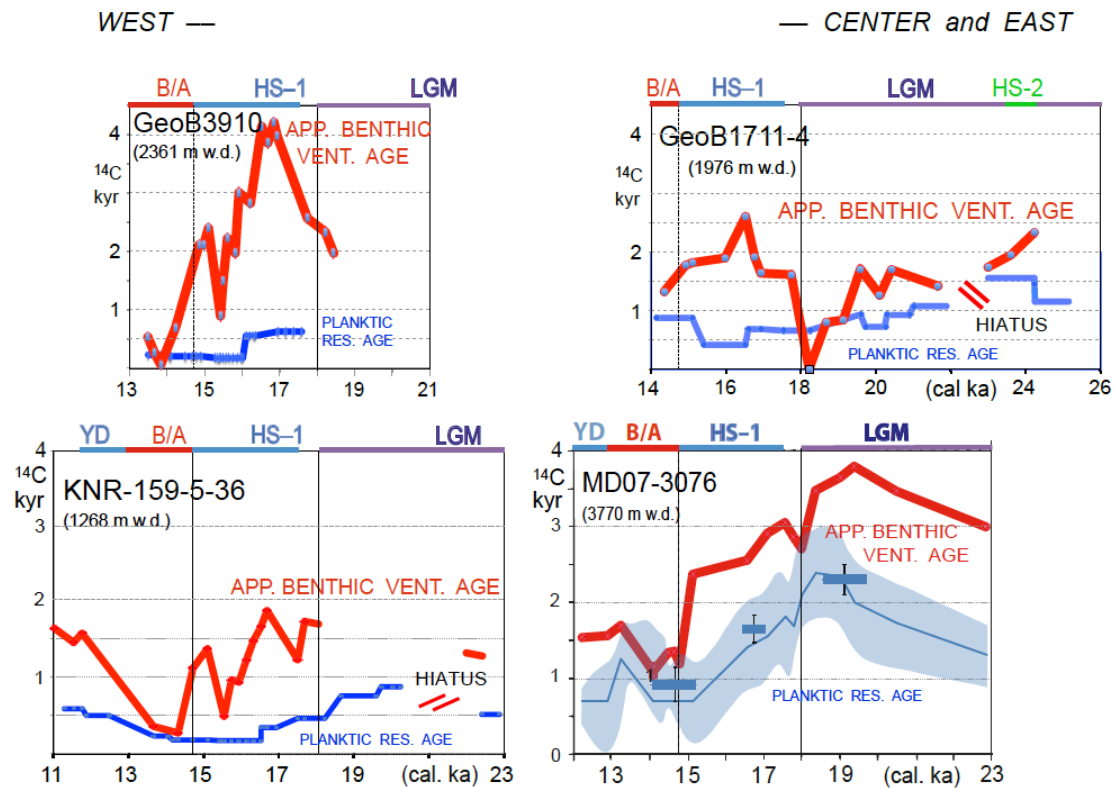


Fig. S4c. SOUTH PACIFIC SITES

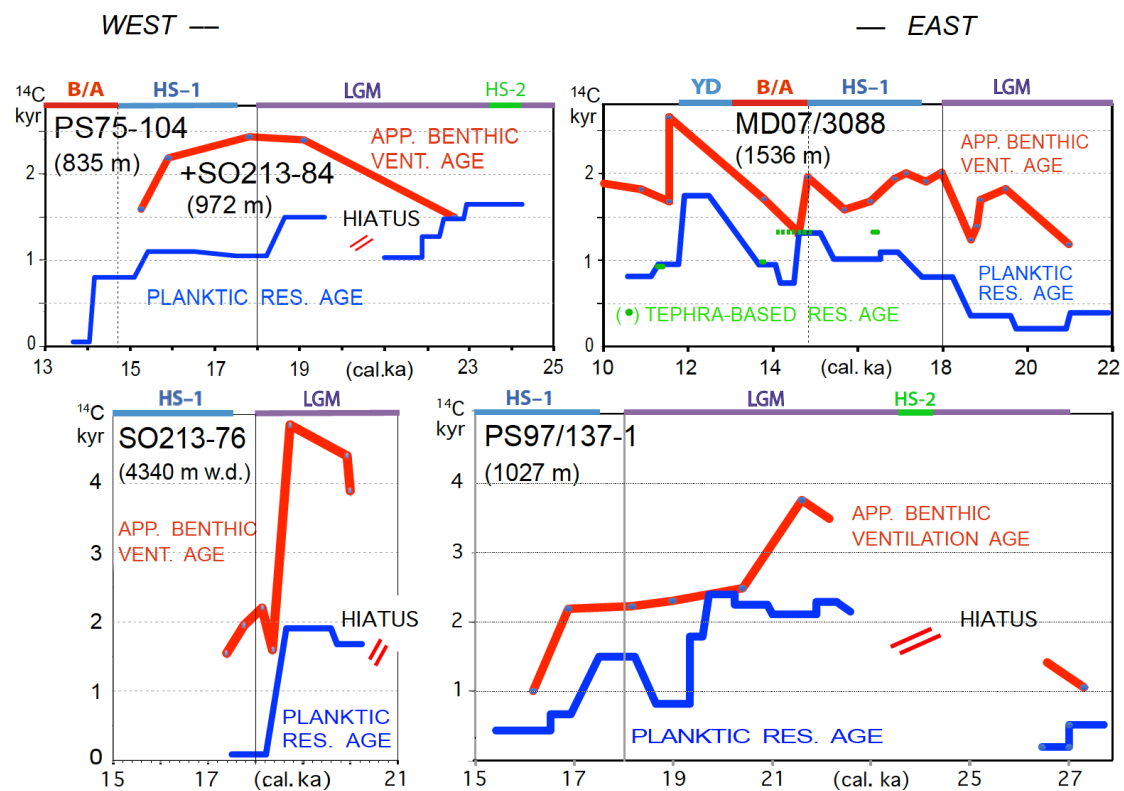


Fig. S4d. NORTH PACIFIC SITES  
*WEST and SOUTH CHINA SEA —*

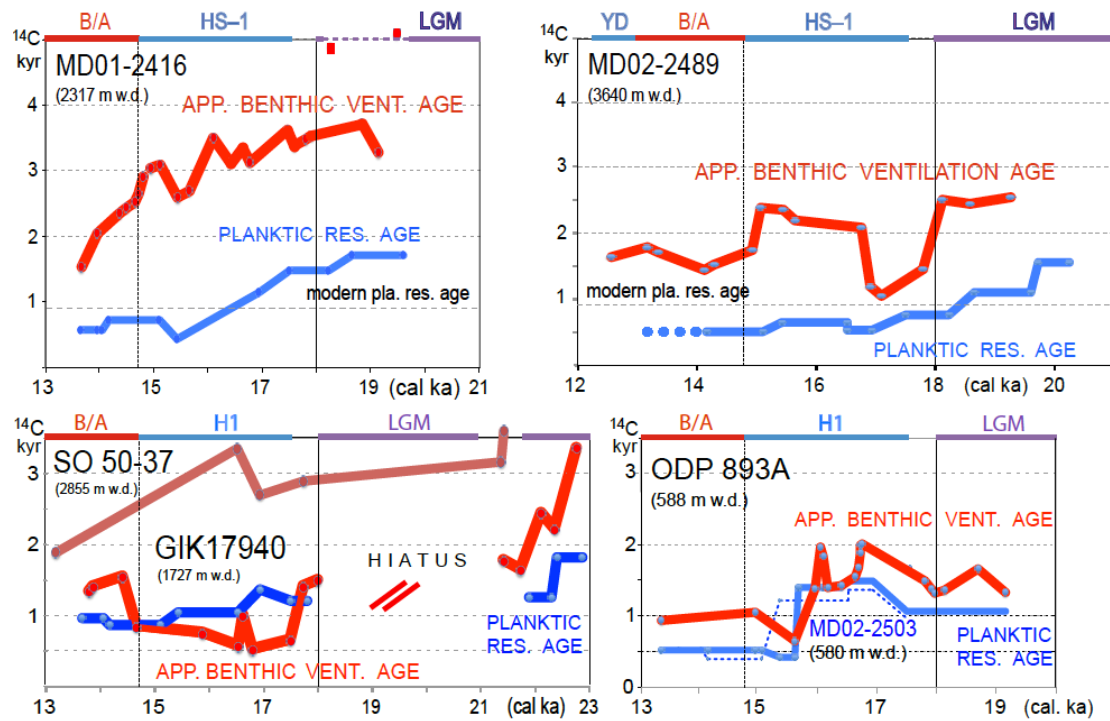
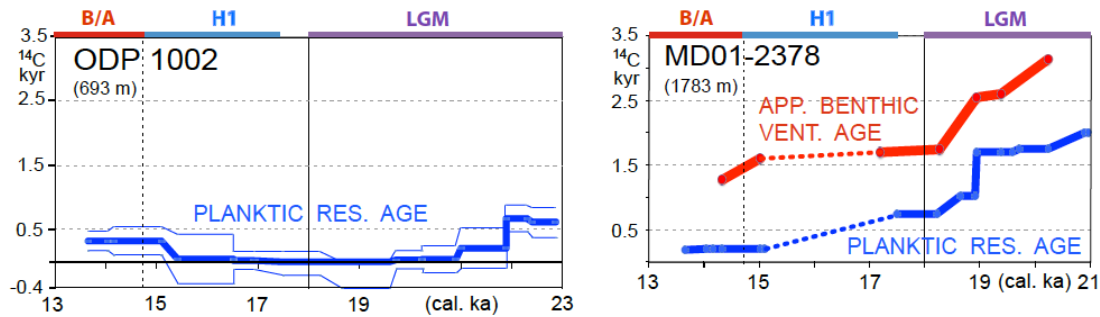


Fig. S4e. SITES in the EQUATORIAL OCEAN

## CARIACO BASIN —

— SOUTHERN TIMOR SEA



1402    **Supplementary Materials**

1403

1404    SUPPLEMENTARY FIGURE CAPTIONS

1405    ¶ Fig. S1. Individual atmospheric  $^{14}\text{C}$  ages and error bars of Lake Suigetsu plant  
1406    macrofossils 15–27 cal. ka vs. U/Th-based model age (blue dots; Bronk Ramsey et al.,  
1407    2012).  $^{14}\text{C}$  plateaus longer than 250 yr are outlined by a suite of labeled horizontal  
1408    boxes that envelop scatter bands of largely constant  $^{14}\text{C}$  ages. Red dots and black  
1409    circles in Fig. 1a display  $^{14}\text{C}$  ages of Hulu stalagmites. Similar to Suigetsu  $^{14}\text{C}$  ages  
1410    those of Hulu Cave also show a suite of  $^{14}\text{C}$  plateaus (red boxes) tentatively assigned in  
1411    this figure, plateaus that are shorter than Suigetsu-based plateaus and occupy slightly  
1412    different age ranges.

1413

1414 ✓ Fig. S2. Location and water depths of sediment cores with age control based on  $^{14}\text{C}$   
1415 plateau tuning.  $^{14}\text{C}$  reservoir ages of cores labeled with 'w' are derived from samples  
1416 with paired wood chunks and planktic foraminifers.

1417

1418

1419 ✓ Fig. S3. (a) Global distribution of  $^{14}\text{C}$  reservoir ages obtained by  $^{14}\text{C}$  plateau tuning  
1420 technique for late LGM surface waters, (b) intermediate waters (100–1800 m w.d.) and  
1421 (c) for ocean deep waters (>1800 m w.d. and Site GIK 23074 at 1157 m in the  
1422 Norwegian Sea). (d)  $^{14}\text{C}$  reservoir ages of LGM surface waters modeled by Muglia et al.  
1423 (2018) for sites with plankton-based age values.

1424

1425

1426 ✓ Fig. S4. Centennial-to-millennial-scale temporal and spatial variations in planktic (pla.)  
1427 reservoir (res.) and (raw = uncorrected) apparent (app.) benthic  $^{14}\text{C}$  ventilation (vent.)  
1428 ages recorded at 18/20 key sites in the Atlantic (S4 a, b, e), Pacific (S4 c, d), and Indian  
1429 (S4 e). Site locations are given in Fig. S2. Stratigraphic units are marked on top of each  
1430 diagram: Younger Dryas (YD), Bølling-Allerød (B/A) Heinrich Stadial 1 (HS-1), Last  
1431 Glacial Maximum (LGM), and Heinrich Stadial 2 (HS-2).

1432 *Origin and various features characteristic of  $^{14}\text{C}$  records:* About 50% of all planktic and  
1433 ('raw') benthic  $^{14}\text{C}$  records already were published in Sarnthein et al. (2015). However,  
1434 the cal. age of all records originally based on microscopy-based varve counts was now  
1435 converted into U/Th-based model ages (Bronk-Ramsey et al., 2012). Planktic  $^{14}\text{C}$   
1436 reservoir ages of Core GIK23074 are now supplemented by benthic ventilation ages.  
1437 Planktic  $^{14}\text{C}$  reservoir ages of SHAK06-5K are detailed in Ausin et al. (2019, in prep.).  
1438 Benthic ventilation ages plotted for SHAK06-5K are matched from neighbor core MD99-

1439 2334K (Skinner et al., 2014) the stratigraphy and  $^{14}\text{C}$  reservoir ages of which are closely  
1440 correlated by means of narrow-spaced suites of  $^{14}\text{C}$  ages. To show an example, ‘raw’  
1441 benthic ventilation ages in Core MD08-3180 are recalculated into ‘actual’ ventilation  
1442 ages (Balmer and Sarnthein, 2018) that incorporate past changes in atmospheric  $^{14}\text{C}$   
1443 concentration between the time of deep-water formation and the local growth of benthic  
1444 foraminifers. South Atlantic  $^{14}\text{C}$  records GeoB3910, GeoB1711-4, and KNR-159-5-36  
1445 (data slightly supplemented) are from Balmer et al. (2016), now however, with cal. ages  
1446 converted into U/Th based model ages. The same applies to MD07-3076, where the  
1447 continuous planktic and benthic  $^{14}\text{C}$  records are from Skinner et al. (2010), corroborated  
1448 by three blue bars reflecting the extent of planktic  $^{14}\text{C}$  plateaus tuned to atmospheric  
1449 plateaus no. 1, 2b, and 4. South Pacific  $^{14}\text{C}$  records PS75-104, SO213-76, MD07-3088,  
1450 and PS97-137-1 are from Küssner et al., 2018 and 2019, in prep.). Planktic and benthic  
1451  $^{14}\text{C}$  records of neighbor cores GIK17940 and SO50-37, PS75-104 and SO213-84, and  
1452 ODP893A and MD02-2503 each are plotted on joint graphs, paired records that are  
1453 obtained from small-scale sea regions with a common level of planktic  $^{14}\text{C}$  reservoir  
1454 age. Benthic  $^{14}\text{C}$  ages of SO50-37 and SO213-84 are from Ronge et al. (2016), those of  
1455 MD07-3088 from Siani et al. (2013).